Journal of Catalysis 274 (2010) 228–238

Contents lists available at ScienceDirect

Journal of Catalysis

journal homepage: www.elsevier.com/locate/jcat

Preparation of supported Pt–Co alloy nanoparticle catalysts for the oxygen reduction reaction by coverage with silica

Sakae Takenaka [a,*], Akiko Hirata [a], Eishi Tanabe [b], Hideki Matsune [a], Masahiro Kishida [a]

[a] Department of Chemical Engineering, Graduate School of Engineering, Kyushu University, Moto-oka 744, Nishi-ku, Fukuoka 819-0395, Japan
[b] Hiroshima Prefectural Technology Research Institute, Kagamiyama 3-13-26, Higashi-Hiroshima, Hiroshima 739-0046, Japan

ARTICLE INFO

Article history:
Received 6 May 2010
Revised 2 July 2010
Accepted 3 July 2010
Available online 4 August 2010

Keywords:
Pt–Co alloy catalysts
Silica coating
Polymer-electrolyte fuel cells
Oxygen reduction reaction

ABSTRACT

Pt-based alloy catalysts such as carbon black-supported Pt–Co catalysts (Pt–Co/CB) are used in the oxygen reduction reaction in polymer-electrolyte fuel cells (PEFCs) and are generally treated at high temperatures to allow for alloy formation. However, treatment of these catalysts at high temperatures results in serious aggregation of alloy particles. In this study, a Pt–Co/CB catalyst was covered with silica layers to inhibit the aggregation of alloy particles during treatment of the catalyst at high temperature for alloy formation. Coverage of Pt–Co/CB with silica promoted Pt–Co alloy formation with a high alloying degree and a small particle size, whereas the alloying degree of Pt–Co alloys in Pt–Co/CB without silica-coating was low, and these alloy particles were seriously aggregated during treatment at high temperature. These silica-coated Pt–Co/CB catalysts showed high activity and excellent durability for the oxygen reduction reaction.

1. Introduction

Polymer-electrolyte fuel cells (PEFCs) have been recognized as promising power sources for zero-emission portable electronics and automobiles. Carbon-supported Pt metal catalysts have been used as catalysts for the oxygen reduction reaction (ORR) at the cathode and for the hydrogen oxidation reaction (HOR) at the anode in PEFCs. The sluggish rate of the ORR on Pt catalysts compared with the rate of the HOR results in a high loading of Pt metal at the cathode. In addition, the Pt catalysts at the cathode should work under severe conditions such as high temperature, low pH, high humidity, an oxygen atmosphere and high potential. Under these conditions, the Pt metal particles on the carbon supports grow in size because of the aggregation of Pt metal particles [1] and because of Ostwald ripening, i.e., dissolution of the cationic Pt species from the small Pt metal particles and redeposition of the cationic Pt species on large metal particles [2,3]. Pt loading at the cathode in the PEFCs should be higher because of the deactivation of the catalysts. However, Pt loading in the PEFCs should be as low as possible for the commercialization of PEFCs because of the high cost of Pt. Recently, many research groups have developed Pt-based alloy catalysts with high activity for the ORR such as Pt–Co, Pt–Ni, Pt–Cu and Pt–Pd [4,5]. Among these Pt-based alloy catalysts, Pt–Co alloy has been the most extensively studied [6–11]. The Pt loading in the catalysts at the cathode can be reduced if Pt–Co alloys are used as catalysts for the ORR since the catalytic activity of the Pt–Co alloys for the ORR, based on the mass of Pt, is higher than that of pure Pt.

Alloy catalysts have been used in many catalytic reactions in addition to PEFCs. For example, Pt–Ru alloy catalysts at anode for the HOR in PEFCs show high tolerance to CO impurity [12] and Pd–Ni alloy catalysts catalyze methane decomposition to form hydrogen and carbon nanofibers [13]. In general, catalysts containing two metal components should be treated at high temperatures to allow alloy formation. Carbon-supported Pt–Co alloy electrocatalysts for the ORR have been also prepared by the addition of Co species on carbon-supported Pt metal catalysts and then alloying at temperatures higher than 973 K in inert gas or hydrogen [14,15]. However, the alloy particles in these catalysts easily aggregate to form larger particles during treatment at high temperatures. To prepare Pt-based alloy catalysts for the ORR in PEFCs, the catalysts are sometimes prepared by the reduction of metal precursors with chemical reductants such as $NaBH_4$ at low temperatures instead of catalyst treatment in hydrogen at high temperatures [16–18]. However, the alloying degree of the catalysts obtained in this way is not always high. The catalytic performance of the alloy catalysts strongly depends on their alloying degree. The aggregation of these alloy particles in the catalysts during treatment at high temperatures should therefore be inhibited to prepare alloy particles with a small size and a high alloying degree.

We have previously prepared metal nanoparticles of Ni and Pt enclosed within spherical silica particles [19,20]. These metal particles in the catalysts can catalyze the combustion of light alkanes and partially oxidize methane to form synthesis gas since the silica

* Corresponding author. Fax: +81 92 802 2752.
E-mail address: takenaka@chem-eng.kyushu-u.ac.jp (S. Takenaka).

0021-9517/$ - see front matter © 2010 Elsevier Inc. All rights reserved.
doi:10.1016/j.jcat.2010.07.005

layers that are wrapped around the metal particles are porous. The metal particles in the catalysts show high durability to sintering even at high temperatures because the metal particles that are covered with silica are not in direct contact with the other metal particles. In addition, we have applied carbon-supported Pt metal covered with silica layers a few nanometers thick as catalysts for the ORR in PEFCs [21,22]. The silica-coated Pt electrocatalysts show high activity for the ORR despite the coverage of Pt metal with the silica insulator. Coverage of the Pt catalysts with silica layers improves the stability of the Pt metal during electrochemical reactions. The silica layers that are wrapped around the Pt metal particles prevent the diffusion of cationic Pt species, which originate from the Pt metal, out of the catalysts. Therefore, the silica-coated Pt catalysts show excellent durability for the ORR. Based on our previous study, we expect that the silica-coating technique will enable us to prepare Pt-based alloy catalysts with a small size and a high alloying degree for the ORR in PEFCs.

In this study, carbon black-supported Pt–Co catalysts were covered with silica layers. The morphology and structure of the metal species in the silica-coated Pt–Co catalysts were examined by transmission electron microscopy (TEM) and X-ray absorption spectroscopy. Furthermore, the catalytic activity and stability of the silica-coated Pt–Co catalysts for the ORR were examined.

2. Experimental

2.1. Catalyst preparation

Carbon black (denoted as CB, Vulcan XC-72 supplied from CABOT. Co.) was impregnated into ethylene glycol containing the desired amounts of H_2PtCl_6 and $CoCl_2$ [23]. The pH of the solution was adjusted to 13 by the addition of NaOH. The solution thus obtained was refluxed at 443 K for 4 h and then filtered. Finally, the samples were reduced with hydrogen at 623 K for 2 h. The CB-supported Pt–Co is denoted as Pt–Co/CB, hereafter.

The coverage of Pt–Co/CB with silica was performed by the successive hydrolysis of 3-aminopropyl-triethoxysilane (APTES) and tetraethoxysilane (TEOS) [24,25]. Pt–Co/CB was immersed into a mixed solution of ethanol and water. APTES and triethylamine, which worked as catalysts for the hydrolysis of APTES and TEOS, were added to the solution. After stirring this solution for 30 min at 353 K for the hydrolysis of APTES, TEOS was added and the solution was stirred. After filtration, the obtained sample was dried in air at 353 K. These Pt–Co catalysts with or without silica were treated at 623 K in hydrogen and further treated at 773 K or 973 K in Ar for 4 h to allow for alloy formation. The silica-coated Pt–Co/CB is denoted as SiO_2/Pt–Co/CB. The treatment temperature for these Pt–Co catalysts in Ar is shown in parenthesis after the catalyst name, for example, SiO_2/Pt–Co/CB treated at 973 K is denoted as SiO_2/Pt–Co/CB (973 K).

2.2. Characterization of the catalysts

Transmission electron microscopy (TEM) images of the catalysts were recorded with a JEOL JEM-200CX instrument. The Pt–Co catalysts were dispersed in iso-propanol, and the solution was mixed ultrasonically at room temperature. A part of this solution was dropped onto a grid for the measurement of TEM images.

X-ray absorption near-edge structure (XANES) and extended X-ray absorption fine structure (EXAFS) measurements were taken at the Photon Factory in the Institute of Materials Structure Science for High Energy Accelerator Research Organization, Japan (Proposal No. 2009G050). Co K-edge and Pt L_{III}-edge XANES/EXAFS spectra were measured in transmission mode at room temperature at beam line BL-9C with a Si(1 1 1) two crystal monochromator. The Pt–Co catalysts were treated in hydrogen at 623 K and further treated at 773 or 973 K in Ar before the XANES and EXAFS measurements. The catalyst samples were packed in a polyethylene bag under an Ar atmosphere. Analysis of the EXAFS data was performed using an EXAFS analysis program, REX (Rigaku Co.). A Fourier transformation of the k^3-weighted EXAFS oscillations was performed over the k range from 4 to 15.5 $Å^{-1}$. Inversely Fourier-transformed data for the Fourier peaks was analyzed using a curve-fitting method including phase shift and amplitude functions derived from FEFF 8.0 [26].

2.3. Electrochemical measurements

Electrochemical measurements were carried out using a three-compartment electrochemical cell with a Pt mesh and a saturated Ag/AgCl electrode serving as the counter and reference electrodes, respectively. All potentials are given relative to the reversible hydrogen electrode (RHE). A glassy carbon disk electrode (5 mm diameter) was used as a substrate for the catalysts and polished to a mirror finish. Catalyst ink was prepared by ultrasonically blending 20 mg of the catalysts and 10 ml of methanol. A 20 μl aliquot of this ink was deposited on a glassy carbon disk and dried at 333 K. Twenty microliters of a 1 wt% Nafion solution diluted with methanol was dropped onto the catalysts to ensure the attachment of the catalysts to the disk. The potential of the catalysts was cycled between 0.05 V and 1.0 V vs. RHE in N_2-purged 0.1 M $HClO_4$ at 333 K to perform accelerated durability tests for the catalysts [27,28]. After potential cycling, we measured cyclic voltammograms (CVs) for the Pt–Co catalysts in N_2-purged 0.1 M $HClO_4$ in the potential range of 0.05–1.20 V. A voltammogram for desorption of underpotentially deposited hydrogen was used to evaluate the electrochemically active surface area (ECSA) for Pt–Co catalysts on the electrode. The value of 210 μC cm-Pt^{-2} was used for determining the ECSA from the adsorbed hydrogen.

A membrane-electrode assembly (MEA) for a PEFC single cell (Electrochem. Co., EFC-05-02) was prepared as follows. Pt–Co/CB and SiO_2/Pt–Co/CB electrocatalysts were used for the cathode and a Pt/CB catalyst for the anode. Catalyst ink was prepared by ultrasonically mixing the catalysts, 2-propanol and diluted Nafion solution (5 wt% Nafion). The catalyst ink was painted onto the surface of wet-proofed carbon paper (Toray Co.) as a gas diffusion layer. A MEA with an area of 5 cm^2 was fabricated by hot pressing the cathode and anode onto Nafion 117 at 403 K and 10 MPa for 3 min. For all the single cell tests in this study, the fuel gas (hydrogen) and the oxidant (oxygen) were humidified at 353 K before being fed into the cells. The cells were operated at 353 K, and the operating pressure was atmospheric pressure.

3. Results and discussion

3.1. Characterization of Pt–Co catalysts

Fig. 1 shows a typical TEM image and the size distribution of the metal particles for Pt–Co/CB (573 K). The particle size distribution was evaluated from the TEM images of the catalysts. The amount of Pt and Co loading in Pt–Co/CB (573 K) was estimated by X-ray fluorescence spectroscopy and found to be 8.1 and 2.2 wt% (mole ratio of Pt/Co = 1.1), respectively. Many metal particles were supported on the CB supports, and their diameters ranged from 1 to 3 nm. The average particle size of the metals in the catalysts was estimated to be 1.7 nm. The Pt–Co/CB (573 K) was treated at 773 or 973 K in Ar or covered with silica layers, followed by treatment at 773 or 973 K in Ar.

Fig. 2 shows TEM images of Pt–Co/CB (773 K) and Pt–Co/CB (973 K). The particle size distribution of the metals in these

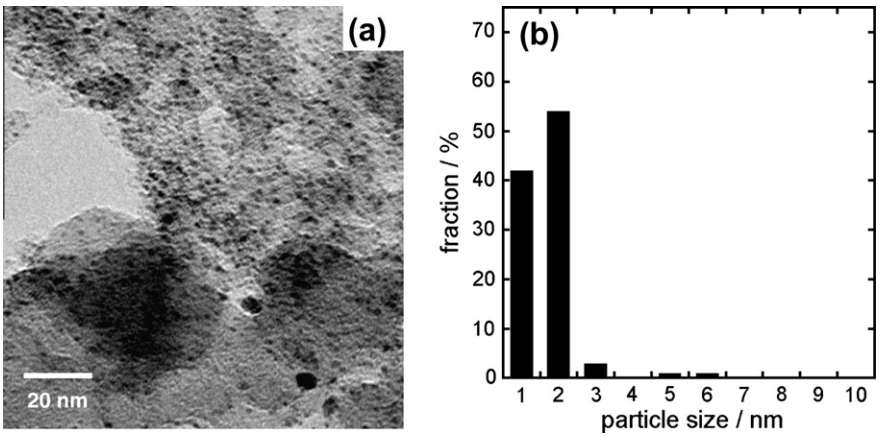

Fig. 1. TEM image and particle size distribution of metals for Pt–Co/CB (573 K).

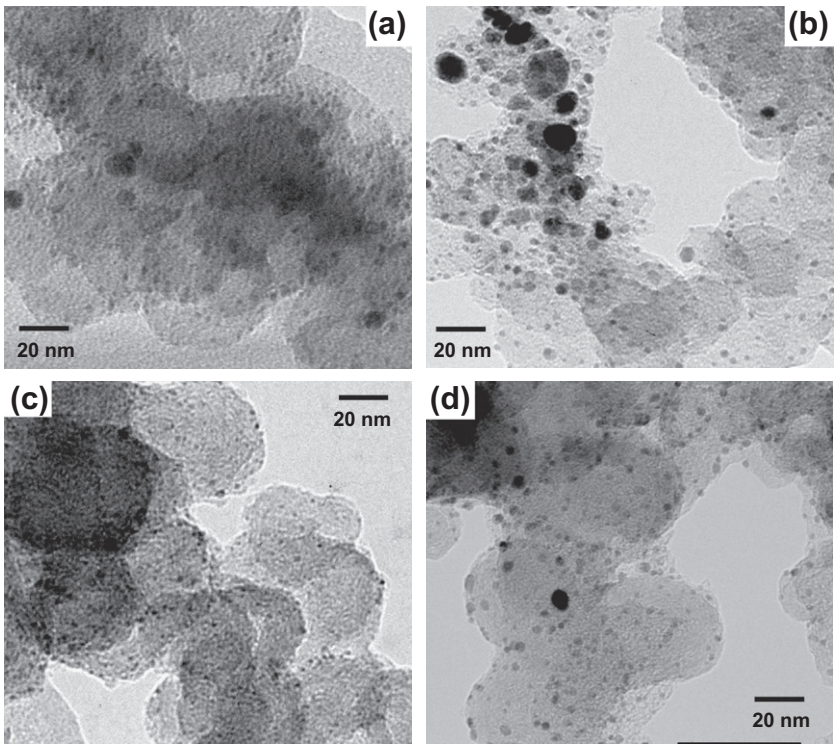

Fig. 2. TEM images of Pt–Co/CB (773 K) (a), Pt–Co/CB (973 K) (b), SiO_2/Pt–Co/CB (773 K) (c) and SiO_2/Pt–Co/CB (973 K) (d).

catalysts is shown in Fig. 3. In the TEM image for Pt–Co/CB (773 K), many metal particles were observed on the CB supports. The diameter of the metal particles in Pt–Co/CB (773 K) ranged from 1 to 6 nm, and the average particle size was 2.4 nm, which is slightly larger than that for Pt–Co/CB (573 K). The metal particle aggregation in Pt–Co/CB was further promoted during treatment at 973 K. As shown in the TEM image for Pt–Co/CB (973 K) in Fig. 2b, the size of many metal particles ranged from 2 to 5 nm, but the diameters of the aggregated metal particles were frequently larger than 6 nm. Therefore, the average particle size of metals in Pt–Co/CB increased from 2.4 nm to 4.8 nm after treatment at 973 K. These results indicated that the metal particles in Pt–Co/CB are seriously aggregated at high catalyst treatment temperatures.

TEM images and the particle size distribution of the metals in SiO_2/Pt–Co/CB are shown in Figs. 2 and 3, respectively. Most of the metal particles in the TEM image of SiO_2/Pt–Co/CB (773 K) are only a few nanometers in diameter. The particle size of the metals in the catalysts ranges from 1 to 5 nm, as shown in Fig. 3c, and the average diameter of the metal particles is 1.9 nm, which is similar to that of Pt–Co/CB (573 K). In addition, the fraction of metal particles in SiO_2/Pt–Co/CB (773 K) that are 1–2 nm in diameter is significantly higher than that for Pt–Co/CB (773 K). These results imply that the silica added to Pt–Co/CB prevents the sintering of metal particles during treatment at 773 K [29]. However, silica was not observed in the TEM image for SiO_2/Pt–Co/CB. The amount of silica loading in SiO_2/Pt–Co/CB (773 K) was estimated by inductively coupled plasma emission spectroscopy (ICP-AES) to be 15 wt%. The presence of silica could not be confirmed by TEM images because of the low loading of silica in the catalysts. The particle size distribution of metals in SiO_2/Pt–Co/CB did not change appreciably after treatment at 973 K, as shown in Figs. 2 and 3d. Many metal particles smaller than 3 nm are present in the TEM image of SiO_2/Pt–Co/CB (973 K), and the average

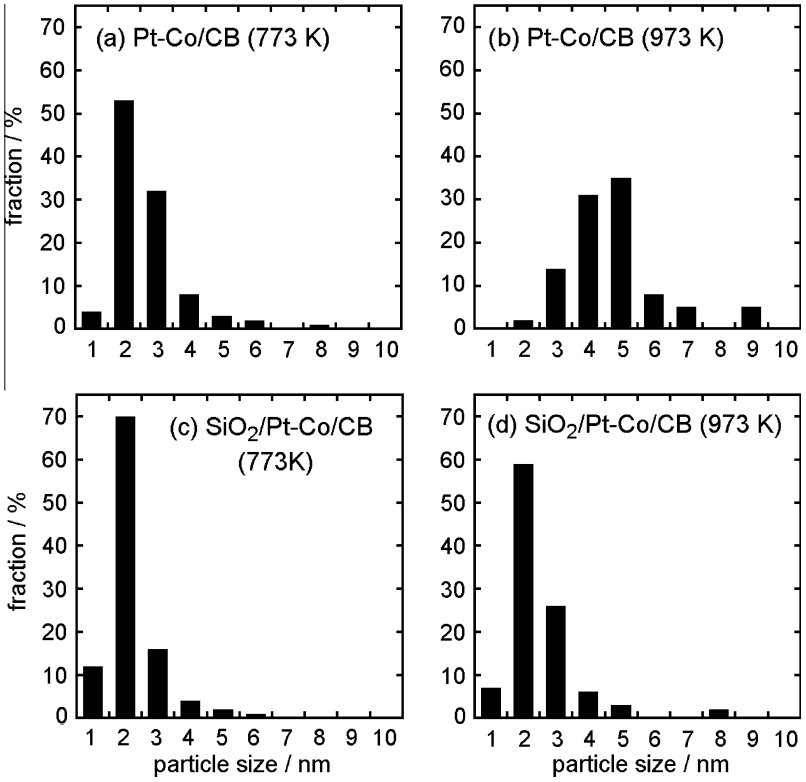

Fig. 3. Particle size distribution for fresh Pt–Co/CB and fresh SiO_2/Pt–Co/CB treated at 773 K and 973 K.

particle size is estimated to be 2.6 nm. The particle size distribution for SiO_2/Pt–Co/CB slightly shifted toward larger sizes as the treatment temperature was increased from 773 to 973 K, but the increase in particle size for SiO_2/Pt–Co/CB was negligible compared to that for Pt–Co/CB. Therefore, we can conclude that the coverage of Pt–Co/CB with silica inhibits the aggregation of metal particles during treatment of the catalysts at high temperatures. The specific surface areas of Pt–Co/CB and SiO_2/Pt–Co/CB were estimated by adsorption of N_2 at 77 K. The specific surface areas of Pt–Co/CB (773 K), Pt–Co/CB (973 K), SiO_2/Pt–Co/CB (773 K) and SiO_2/Pt–Co/CB (973 K) were 190, 188, 169 and 160 $m^2\ g^{-1}$, respectively. These results indicated that treatment of the catalysts at 973 K did not reduce the surface area of CB support. Thus, the coverage of Pt–Co/CB with silica prevents the aggregation of metal particles rather than the sintering of CB supports.

Fig. 4 shows XRD patterns of Pt/CB, Pt–Co/CB and SiO_2/Pt–Co/CB after treatment at different temperatures. Three peaks in the XRD pattern of Pt/CB are characteristic of face-centered cubic (fcc) crystalline Pt metal, corresponding to the (1 1 1), (2 0 0) and (2 2 0) planes at 2θ values of 39.4°, 46.3° and 67.5°, respectively. In the XRD patterns for all the Pt–Co/CB catalysts, three peaks characteristic of face-centered cubic crystalline Pt were observed, but the peak position for the Pt–Co/CB catalysts was at higher 2θ values compared to those of Pt/CB, i.e., the peak due to the (1 1 1) plane for Pt–Co/CB (573 K), Pt–Co/CB (773 K) and Pt–Co/CB (973 K) was positioned at 2θ values of 40.1°, 40.3° and 40.0°, respectively. No reflection arising from a superlattice such as a face-centered tetragonal alloy phases was present in the XRD patterns for the Pt–Co catalysts [10,30]. These results indicate the formation of disordered Pt–Co alloys involving the incorporation of Co atoms in the face-centered cubic crystalline of Pt metal. Additional two peaks were observed at around 44.0° and 51.3° in the XRD pattern of Pt–Co/CB (973 K). These peaks could be due to crystalline Co or Pt–Co alloys with high Co/Pt mole ratios [30,31]. On the other hand, only peaks due to the face-centered cubic crystalline Pt metal were found in the XRD patterns of both the SiO_2/Pt–Co/CB catalysts, and these peaks were also present at higher 2θ values compared to crystallite Pt. The peak for the (1 1 1) plane was

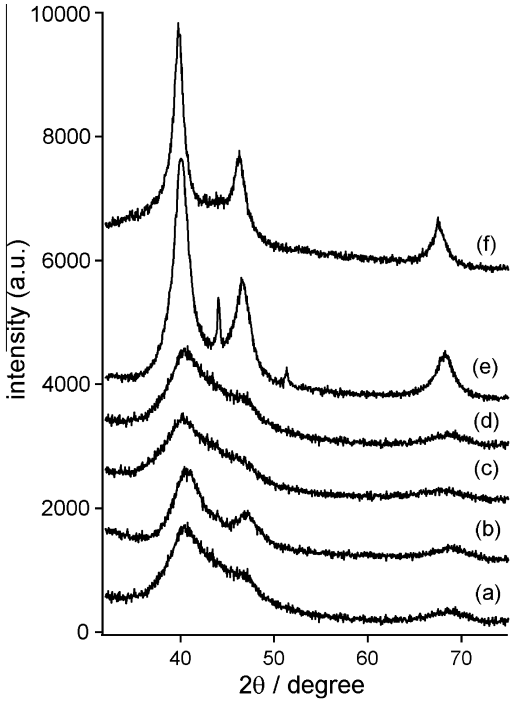

Fig. 4. XRD patterns of SiO_2/Pt–Co/CB (773 K) (a), SiO_2/Pt–Co/CB (973 K) (b), Pt–Co/CB (573 K) (c), Pt–Co/CB (773 K) (d), Pt–Co/CB (973 K) (e) and Pt/CB (f).

present at 2θ values of 40.4° and 40.6° for SiO_2/Pt–Co/CB (773 K) and SiO_2/Pt–Co/CB (973 K), respectively, indicating the formation of disordered Pt–Co alloys. It should be noted that the peaks due to the Pt–Co alloys in the XRD patterns of SiO_2/Pt–Co/CB shifted to higher 2θ values at higher catalyst treatment temperatures, while the peak position in the XRD patterns of the Pt–Co/CB catalysts did not strongly depend on the treatment temperature of the catalysts. Coverage of Pt–Co/CB with silica improves the alloying degree of the Pt–Co alloys during the treatment of the catalysts at high temperatures. Additionally, the peaks due to the Pt–Co alloys for Pt–Co/CB became sharper at higher catalyst treatment temperatures. In contrast, the peak width for the Pt–Co alloys in the SiO_2/Pt–Co/CB catalysts did not change appreciably with an increase in the catalyst treatment temperature. Therefore, coverage of the Pt–Co/CB catalysts with silica promotes the formation of Pt–Co alloys with a high alloying degree and a small particle size.

Fig. 5 shows Pt L_{III}-edge XANES spectra and Fourier transforms of k^3-weighted Pt L_{III}-edge EXAFS spectra for Pt foil, Pt–Co/CB and SiO_2/Pt–Co/CB. XANES spectra of both the Pt–Co/CB were very similar in shape to that of Pt foil, as shown in Fig. 5a. Therefore, most of the Pt species in both the Pt–Co/CB were present in the metallic state [32,33]. The absorption at around 11,565 eV in the Pt L_{III}-edge XANES spectra, which is known as a white line, corresponds to an electron transition from $2p_{3/2}$ to 5d, and the magnitude of the white line is related to the 5d-electron vacancies [34,35]. We found that the intensity of the white line for the XANES spectrum of Pt–Co/CB (773 K) was slightly smaller than that for Pt foil. Alloying of Co with Pt metal thus results in a more occupied Pt 5d electronic state [36]. The intensity of the white line in the XANES spectra of the Pt–Co/CB catalysts did not depend on the catalyst treatment temperature suggesting that the alloying degree of the Pt–Co alloys in Pt–Co/CB did not improve significantly with the treatment temperature of the catalysts. Earlier XRD studies on Pt–Co/CB also showed the same results. The XANES spectrum of SiO_2/Pt–Co/CB (773 K) resembles that of Pt–Co/CB (773 K) in shape, i.e., slightly lower intensity of the white line in the XANES spectrum of SiO_2/Pt–Co/CB (773 K) compared with that for Pt foil. In contrast, the white line in the XANES spectrum of SiO_2/Pt–Co/CB decreased in intensity after treatment at 973 K. Therefore, the alloying degree of the Pt–Co alloys in SiO_2/Pt–Co/CB increased with an increase in the catalyst treatment temperature.

Fourier transforms of the Pt L_{III}-edge EXAFS spectra (RSFs, radial structure functions) for Pt–Co/CB and SiO_2/Pt–Co/CB clarified the structure of the metal particles. A strong peak is present in the R range from 2.2 to 3.0 Å in the RSFs for all the Pt–Co catalysts, as shown in Fig. 5c and d. The peaks in the RSFs for Pt–Co/CB (773 K), Pt–Co/CB (973 K) and SiO_2/Pt–Co/CB (773 K) are all located at around 2.5 Å, whereas the peak is present at a shorter distance (2.4 Å) in the RSF for SiO_2/Pt–Co/CB (973 K). The RSFs for Pt–Co/CB and SiO_2/Pt–Co/CB were inversely Fourier-transformed in the R range from 1.5 to 3.3 Å, and the EXAFS spectra thus obtained were fitted in the k range from 4.5 to 15.0 $Å^{-1}$. The structural parameters

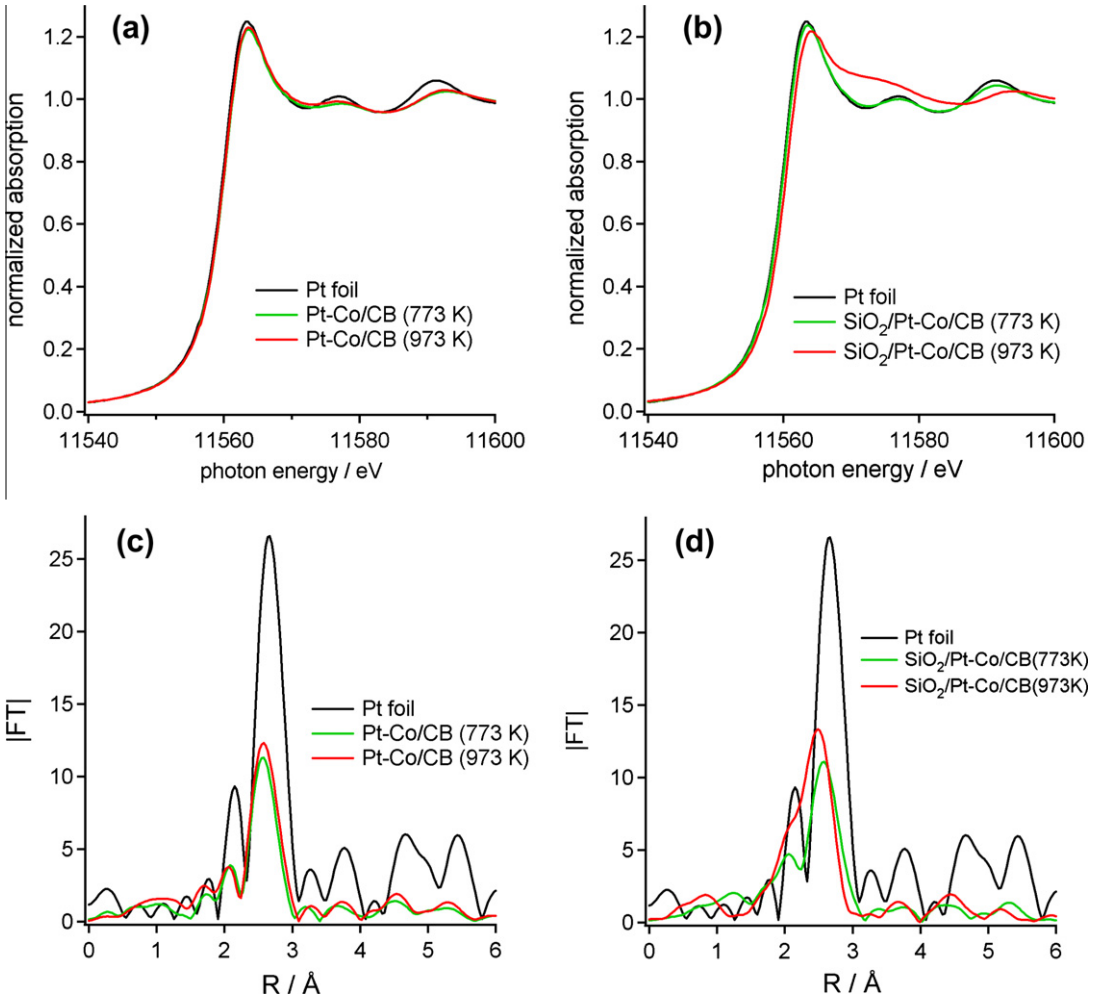

Fig. 5. Pt L_{III}-edge XANES spectra of Pt–Co/CB (a) and of SiO_2/Pt–Co/CB (b) and Fourier transforms of Pt L_{III}-edge k^3-weighted EXAFS spectra of Pt–Co/CB (c) and of SiO_2/Pt–Co/CB (d).

Table 1
Structural parameters of metal species in Pt–Co/CB and SiO_2/Pt–Co/CB estimated by curve-fitting for Pt L_{III}-edge EXAFS.

Catalyst	Shell	CN[a]	R[b] (Å)	σ[c] (Å)
Pt–Co/CB (773 K)	Pt–Pt	7.3 ± 0.4	2.72	0.075
	Pt–Co	0.5 ± 0.1	2.61	0.065
Pt–Co/CB (973 K)	Pt–Pt	9.2 ± 0.5	2.73	0.078
	Pt–Co	0.6 ± 0.1	2.65	0.068
SiO_2/Pt–Co/CB (773 K)	Pt–Pt	6.1 ± 0.2	2.72	0.070
	Pt–Co	1.4 ± 0.1	2.63	0.066
SiO_2/Pt–Co/CB (973 K)	Pt–Pt	5.3 ± 0.2	2.70	0.069
	Pt–Co	3.5 ± 0.2	2.60	0.068

[a] Coordination number.
[b] Interatomic distance.
[c] Debye Waller factor.

estimated by the curve-fitting analyses are listed in Table 1. The EXAFS spectra for all the Pt–Co catalysts could be fitted using two kinds of shell, Pt–Pt and Pt–Co bonds. The coordination numbers of Pt–Pt and Pt–Co for Pt–Co/CB (773 K) were estimated to be 7.3 and 0.5, respectively. The interatomic distance of Pt–Pt in the catalyst (2.72 Å) was shorter than that of Pt–Pt in Pt foil (2.77 Å) indicating the formation of Pt–Co alloys. However, the alloying degree of the Pt–Co alloys in Pt–Co/CB (773 K) was very low because the coordination number of the Pt–Co bond was very low. The ratio of the coordination number for the Pt–Co bond compared to that for the Pt–Pt bond in Pt–Co/CB did not change when the catalyst treatment temperature increased from 773 to 973 K, indicating that the alloying degree of the Pt–Co alloys in Pt–Co/CB (773 K) was similar to that in Pt–Co/CB (973 K), *i.e.* low alloying degree of Pt–Co alloys in these catalysts. The increase in the total coordination number of Pt–Co and Pt–Pt bonds with the treatment temperature of Pt–Co/CB suggests that aggregation of the alloy particles occurred during catalyst treatment at 973 K. The structural parameters of the metal species in SiO_2/Pt–Co/CB (773 K) are very similar to those for Pt–Co/CB (773 K), although the coordination number of Pt–Co for the former catalyst is slightly larger than that for the latter catalyst. When SiO_2/Pt–Co/CB was treated at 973 K, the coordination number of Pt–Co increased and the coordination number of Pt–Pt decreased. It is important to note that the total coordination number of Pt–Pt and Pt–Co in SiO_2/Pt–Co/CB (973 K) was slightly larger than that in SiO_2/Pt–Co/CB (773 K), but it was lower than that in Pt–Co/CB (973 K). Therefore, coverage of Pt–Co/CB with silica promotes Pt–Co alloy formation without aggregation of alloy particles.

Fig. 6 shows Co K-edge XANES spectra and Fourier transforms of the k^3-weighted Co K-edge EXAFS spectra (RSFs) for Co foil, Pt–Co/CB and SiO_2/Pt–Co/CB. A pre-edge peak (denoted as peak A, hereafter) is present at around 7710 eV in the Co K-edge XANES spectra and is assigned to the 1s to 3d transition, while the peak at around 7725 eV (denoted as peak B, hereafter) corresponds to the 1s to hybridized 4s and 4p transition [37,38]. The XANES spectrum of Pt–Co/CB (773 K) resembles that of Pt–Co/CB (973 K) in shape. The intensity of peak B was higher, and the intensity of peak A was slightly lower in the XANES spectra of both the Pt–Co/CB catalysts compared to the corresponding peak intensity in the XANES spectrum of Co foil. The XANES spectra of the Pt–Co/CB prepared in this study are consistent with those of the Pt–Co alloy catalysts previously reported [39,40], indicating that Pt–Co alloys are formed in these Pt–Co/CB catalysts. It has been reported that peak B increases in intensity in contrast to a slight decrease in the intensity of peak A in the XANES spectra of Pt–Co alloys with higher Co content [37]. Therefore, the alloying degree of the Pt–Co alloys in the Pt–Co/CB catalysts did not change when the catalyst treatment temperature increased. The intensity of peak A was smaller, and the intensity of peak B was higher in the XANES spectrum of SiO_2/Pt–Co/CB (773 K) compared with the corresponding peak intensities in the XANES spectra of the Pt–Co/CB catalysts. This feature in the XANES spectrum of SiO_2/Pt–Co/CB (773 K) was enhanced after the catalysts were treated at 973 K, indicating an improvement in the alloying degree of the Pt–Co alloys in the SiO_2/Pt–Co/CB catalysts. As described below, some Co atoms in SiO_2/Pt–Co/CB (773 K) were present in the oxidized state, and some of the oxidized Co species were reduced to the metallic state during catalyst treatment at 973 K. The presence of oxidized Co in the catalysts also increased the intensity of peak B in the Co K-edge XANES spectra [41].

Fourier transforms of Co K-edge EXAFS (RSFs) for Pt–Co/CB and SiO_2/Pt–Co/CB are shown in panels (c) and (d) in Fig. 6, respectively. Strong peaks were observed at 2.2, 4.0 and 4.6 Å in the RSFs for both the Pt–Co/CB, and the position of these peaks was similar to that of Co foil. A peak was also observed at 2.2 Å in the RSF for SiO_2/Pt–Co/CB (773 K). However, the peak for SiO_2/Pt–Co/CB (773 K) was lower in intensity and broader in width compared to that for Pt–Co/CB. This would be because some Co species in the catalysts were oxidized. The peak at 2.2 Å in the RSF of SiO_2/Pt–Co/CB (773 K) was slightly shifted toward a longer distance after treatment at 973 K, implying the formation of Pt–Co alloys with a higher alloying degree.

Table 2 shows the structural parameters of the metal species estimated by curve-fitting for the Co K-edge EXAFS spectra of Pt–Co/CB and SiO_2/Pt–Co/CB. The EXAFS spectra for both the Pt–Co/CB could be fitted by two shells of Co–Co and Co–Pt bonds. The coordination numbers of Co–Co and Co–Pt for Pt–Co/CB (773 K) were estimated to be 6.6 and 0.5, respectively. The ratio of the coordination number of Co–Pt to Co–Co in Pt–Co/CB (773 K) was low despite a molar ratio for Pt/Co of 1.1 for the catalysts, and the ratio of the coordination number did not change during treatment of the catalysts at 973 K. On the other hand, the EXAFS spectra for both the SiO_2/Pt–Co/CB could be fitted by three shells consisting of Co–Co, Co–Pt and Co–O bonds. The coordination number of Co–O in the SiO_2/Pt–Co/CB (773 K) was estimated to be 1.8, and it decreased to 1.1 after treatment of the catalysts at 973 K. Some Co atoms in SiO_2/Pt–Co/CB were present in the oxidized state, and some of the oxidized Co species were reduced to a metallic state during treatment of the catalysts at 973 K. We have previously reported the preparation of Co particles enclosed in spherical silica particles [42]. Some Co atoms in these catalysts were also stabilized in the oxidized state, even after treatment of the catalysts at 1073 K, and the oxidized Co species were atomically dispersed within the silica particles. It is likely that some of the Co atoms in SiO_2/Pt–Co/CB were also present as highly dispersed CoO_x species in the silica layers. The coordination numbers of Co–Co and Co–Pt in SiO_2/Pt–Co/CB (773 K) were estimated to be 2.7 and 1.1, respectively. The ratio of the coordination number of Co–Pt to Co–Co increased after treatment of the catalysts at 973 K. Therefore, we concluded that the coverage of Pt–Co/CB with silica, followed by treatment at 973 K, promotes the formation of a Pt–Co alloy with a high alloying degree.

As described earlier, the alloying degree of the Pt–Co alloys in SiO_2/Pt–Co/CB (973 K) was higher than that in Pt–Co/CB (973 K). For the preparation of Pt–Co/CB, carbon black was impregnated into ethylene glycol containing H_2PtCl_6 and $CoCl_2$, and the solution was refluxed at 443 K. Ethylene glycol as a reductant is not strong enough to reduce $CoCl_2$ to Co metal although H_2PtCl_6 is reduced to Pt metal [43–45]. The Co metal precursors that were supported on CB were reduced to Co metal during treatment of the catalysts with hydrogen at 623 K or under Ar at 773 K. The Co metal precursors were deposited onto the CB supports by increasing the pH of the solution containing $CoCl_2$ and H_2PtCl_6 up to 13 during the preparation of the Pt–Co catalysts. Beard et al. prepared carbon-supported

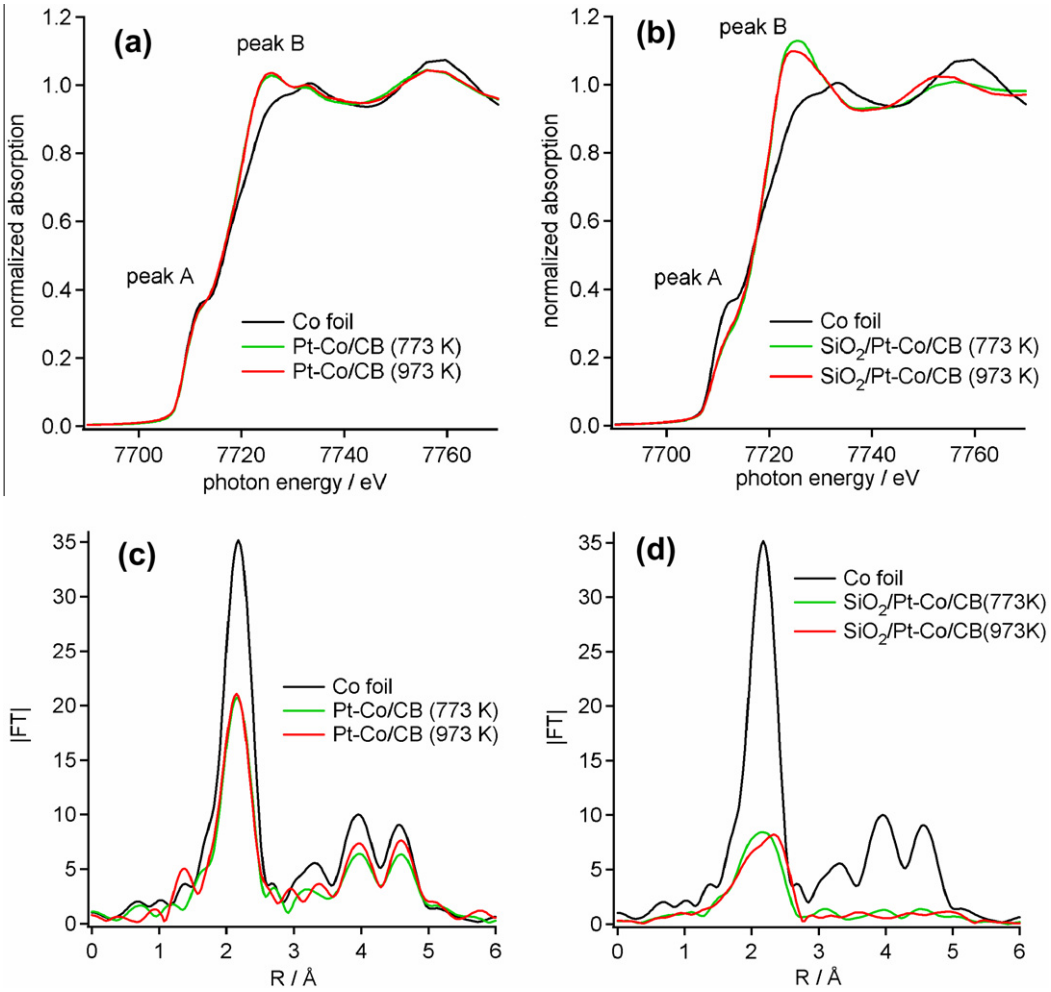

Fig. 6. Co K-edge XANES spectra of Pt–Co/CB (a) and of SiO_2/Pt–Co/CB (b) and Fourier transforms of Co K-edge k^3-weighted EXAFS spectra of Pt–Co/CB (c) and of SiO_2/Pt–Co/CB (d).

Table 2
Structural parameters of metal species estimated by curve-fitting for Co K-edge EXAFS of Pt–Co/CB and SiO_2/Pt–Co/CB.

Catalyst	Shell	CN[a]	R[b] (Å)	σ[c] (Å)
Pt–Co/CB (773 K)	Co–Co	6.6 ± 0.3	2.48	0.070
	Co–Pt	0.5 ± 0.1	2.60	0.065
Pt–Co/CB (973 K)	Co–Co	7.4 ± 0.4	2.48	0.075
	Co–Pt	0.6 ± 0.1	2.62	0.063
SiO_2/Pt–Co/CB (773 K)	Co–O	1.8 ± 0.2	2.08	0.060
	Co–Co	2.7 ± 0.1	2.51	0.070
	Co–Pt	1.1 ± 0.2	2.61	0.070
SiO_2/Pt–Co/CB (973 K)	Co–O	1.1 ± 0.2	2.08	0.062
	Co–Co	2.9 ± 0.1	2.52	0.081
	Co–Pt	2.5 ± 0.2	2.63	0.074

[a] Coordination number.
[b] Interatomic distance.
[c] Debye Waller factor.

Pt–Co catalysts in acid and alkaline aqueous media and found that a higher alloying degree of Pt–Co was obtained using the catalysts prepared in the acid medium [8]. The low alloying degree of the Pt–Co alloys in the catalysts prepared in the alkaline media was due to a poor interaction between Pt metal particles and the Co metal precursors before the reduction of the catalysts at high temperature. The poor interaction between Pt metal and the Co metal precursors promoted the formation of large Co metal particles instead of the formation of Pt–Co alloys during the reduction of the Pt–Co/CB catalysts at high temperatures. The formation of large Co metal particles in Pt–Co/CB retarded the formation of Pt–Co alloys with a high alloying degree. Thus, the alloying degree of aggregated metal particles in Pt–Co/CB was very low even after the catalysts had been treated at 973 K. Coverage of the Pt–Co catalysts with silica layers promotes the formation of Pt–Co alloy particles with a high alloying degree, because the silica-coating prevents the sintering of Co metal particles to form large Co metal particles. Therefore, the alloying degree of the Pt–Co alloys in SiO_2/Pt–Co/CB was higher, and their particles size was smaller compared to those in the Pt–Co/CB catalysts.

3.2. Catalytic performance of Pt–Co catalysts

Fig. 7 shows cyclic voltammograms (CVs) of the Pt–Co/CB and SiO_2/Pt–Co/CB catalysts in N_2-purged 0.1 M $HClO_4$ at 333 K during potential cycling between 0.05 and 1.0 V for the accelerated durability test of the catalysts. Before the CV measurements of the fresh catalysts, ca. 20 cycles of potential cycling were carried out from 0.05 to 1.20 V to obtain reproducible CVs. In the CVs for all the Pt–Co catalysts, two peak couples are observed, and these are assigned to the adsorption and desorption of hydrogen on Pt from 0.05 to 0.3 V and to the oxidation and reduction of Pt from 0.6 to 1.2 V. These are observed despite the coverage of Pt–Co alloys with

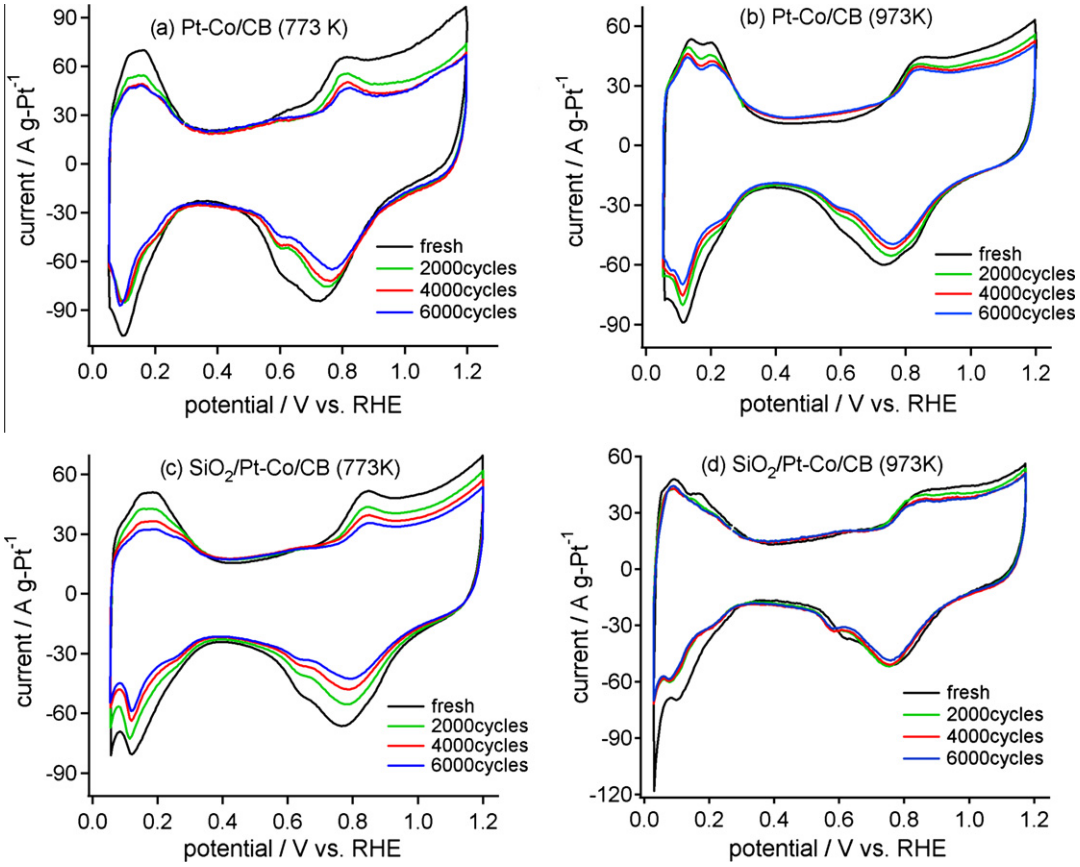

Fig. 7. Cyclic voltammograms of Pt–Co/CB (773 K) (a), Pt–Co/CB (973 K) (b), SiO_2/Pt–Co/CB (773 K) (c) and SiO_2/Pt–Co/CB (973 K) (d) in N_2-purged $HClO_4$ during the potential cycling experiments from 0.05 to 1.0 V at 333 K.

the silica insulator in the CVs of SiO_2/Pt–Co/CB catalysts. Reactant molecules such as water and protons diffuse onto the Pt–Co alloy surface in SiO_2/Pt–Co/CB through the porous silica layers and electrons conduct into the alloys through the exposed CB surface. Protons would also diffuse onto the Pt–Co alloys through water molecules adsorbed on the silica surfaces. Therefore, the SiO_2/Pt–Co/CB is electrochemically active. The intensity of the peaks in the CVs for both the Pt–Co/CB decreases with the number of the potential cycling. This decrease in peak intensity is also observed in the CVs of SiO_2/Pt–Co/CB (773 K) during the accelerated durability test. In contrast, the peak intensity due to Pt metal in the CVs for SiO_2/Pt–Co/CB (973 K) does not change appreciably during the potential cycling experiment. The peak intensity for the SiO_2/Pt–Co/CB (973 K) decreases slightly until 2000 cycles, but then it remains constant. The high alloying degree of Pt–Co alloys results in the excellent durability of the SiO_2/Pt–Co/CB (973 K) catalysts during the durability test [27,28]. Treatment of silica layers at 973 K also contributes to an improvement in the durability of the catalysts. We have previously reported that the coverage of carbon-supported Pt catalysts with silica layers improves the durability of Pt metal during the potential cycling experiment [46]. The durability of the silica-coated Pt catalysts depends on the thickness and density of silica layers. The loading of silica in the highly durable silica-coated Pt catalysts was ca. 40 wt%, and the catalyst was treated at 873 K. The treatment of the silica-coated Pt catalysts at high temperature results in the formation of dense silica layers. The silica loading and the treatment temperature for SiO_2/Pt–Co/CB (773 K) were not high enough to improve the durability of the catalyst during the potential cycling experiment. In contrast, dense silica layers in SiO_2/Pt–Co/CB (973 K) prevent the diffusion of Pt and/or Co species dissolved from Pt–Co alloys out of the catalysts. Thus, the coverage of the Pt–Co catalysts with dense silica layers further improved the durability of the catalysts. As described in the previous study, the Pt catalysts covered with silica layers showed a similar activity for the ORR to the Pt catalysts without silica-coating [22]. Thus, the silica layers, which are wrapped around Pt metal particles, do not prevent the diffusion of reactant molecules such as proton and oxygen, although the diffusion of cationic Pt species

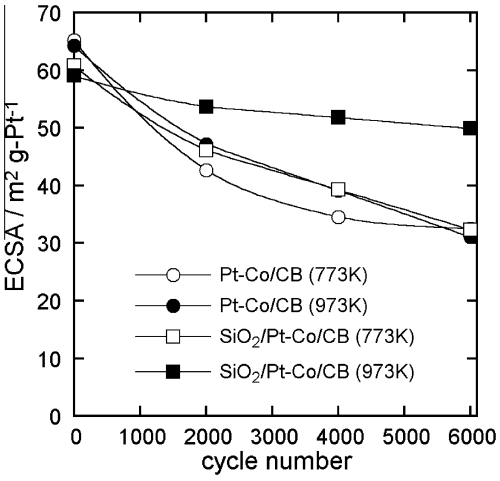

Fig. 8. Changes of ECSAs of Pt in Pt–Co/CB and SiO_2/Pt–Co/CB treated at 773 K and 973 K during the potential cycling experiments.

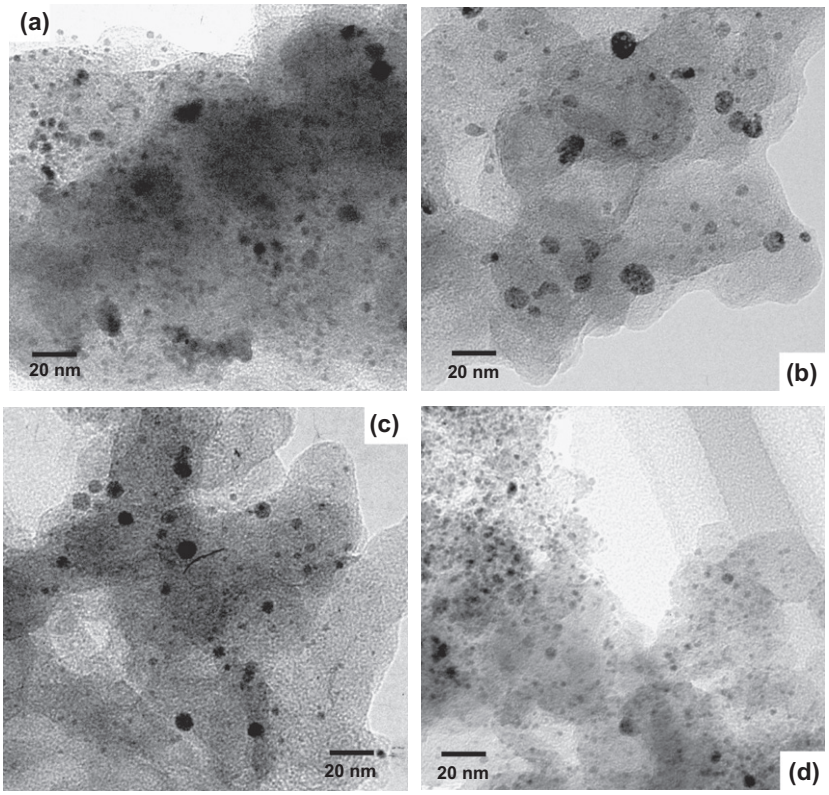

Fig. 9. TEM images of Pt–Co/CB (773 K) (a), Pt–Co/CB (973 K) (b), SiO_2/Pt–Co/CB (773 K) (c) and SiO_2/Pt–Co/CB (973 K) (d) after 6000 cycles of the potential cycling.

dissolved from Pt metal particles out of the catalysts is inhibited by the silica layers. This would be due to difference in size between cationic Pt species and reactant molecules (proton and oxygen), since the cationic Pt species are surrounded with many water molecules under the PEFC cathode conditions. In order to clarify the porous structure of silica layers in the silica-coated catalysts, we performed N_2 adsorption on the catalysts at 77 K, but the thickness of silica layers in the catalysts was too thin to evaluate the porous structure.

Based on the CVs shown in Fig. 7, the electrochemically active surface areas (ECSAs) of Pt in all the Pt–Co catalysts were evaluated. The results are shown in Fig. 8. The ECSAs for Pt–Co/CB (773 K), Pt–Co/CB (973 K) and SiO_2/Pt–Co/CB (773 K) became gradually smaller with an increase in the number of potential cycles and finally decreased to half at 6000 cycles. In contrast, the decrease in the ECSA for SiO_2/Pt–Co/CB (973 K) was not as serious as that of the other catalysts. SiO_2/Pt–Co/CB (973 K) had a ECSA of 50 m^2 g-Pt^{-1} even after 6000 potential cycles.

Fig. 9 shows TEM images of the Pt–Co/CB and SiO_2/Pt–Co/CB catalysts after 6000 potential cycles. The particle size distribution of metals in these Pt–Co catalysts after the potential cycling experiment is shown in Fig. 10. The Pt–Co alloy particles larger than 5 nm in diameter were abundant in the TEM images for the used Pt–Co/CB (773 K), Pt–Co/CB (973 K) and SiO_2/Pt–Co/CB (773 K) catalysts. The particle size of Pt–Co alloys in these catalysts after potential cycling was widely distributed from 2 to 15 nm, as shown in Fig. 10. The fresh catalysts had smaller Pt–Co alloy particles and a narrower particle size distribution compared with the used catalysts (Fig. 3). The average particle size of the Pt–Co alloys changed from 2.4 to 6.3 nm for Pt–Co/CB (773 K), from 4.8 to 7.2 nm for Pt–Co/CB (973 K) and from 1.8 to 6.0 nm for SiO_2/Pt–Co/CB (773 K) during the potential cycling experiment. The low durability of the Pt–Co/CB (773 K), Pt–Co/CB (973 K) and SiO_2/Pt–Co/CB (773 K) catalysts during the potential cycling experiments arises from the low alloying degree of the Pt–Co alloys. In contrast, aggregated Pt–Co alloy particles are scarce in the TEM image for used SiO_2/Pt–Co/CB (973 K), as shown in Fig. 9d. The particle size distribution of the Pt–Co alloys in SiO_2/Pt–Co/CB (973 K) is shifted slightly toward a larger size distribution during the potential cycling experiment as shown in Figs. 3 and 10d, but the increment in alloy particle size in the SiO_2/Pt–Co/CB (973 K) is negligible compared with that in the other catalysts. The higher alloying degree of the Pt–Co alloys and the coverage with dense silica layers result in highly durable SiO_2/Pt–Co/CB (973 K) during the potential cycling experiment [27,28].

The catalytic activity of SiO_2/Pt–Co/CB (973 K) for the oxygen reduction reaction (ORR) was evaluated using a PEFC single cell. Fig. 11 shows polarization curves of PEFC single cells with Pt/CB, Pt–Co/CB (973 K) and SiO_2/Pt–Co/CB (973 K) catalysts at cathode. Pt/CB was always used as a catalyst for the hydrogen oxidation reaction at the anode. The loading of Pt in Pt/CB was 15 wt%, and the average particle size of Pt in the catalyst was 4.2 nm. As shown in Fig. 11, the catalytic activity of Pt–Co/CB (973 K) for the ORR was lower than that of Pt/CB. Because the alloying degree of Pt–Co alloy particles was very low and their particle size was large in the Pt–Co/CB (973 K) catalysts, the catalysts showed lower activity for the ORR than Pt/CB. In contrast, SiO_2/Pt–Co/CB (973 K) showed higher activity for the ORR than the other catalysts, in spite of the coverage with silica layers. The catalytic activity of SiO_2/Pt–Co/CB (973 K) was high even in the region of a low cell voltage. The thickness of silica layers, which were wrapped around Pt–Co alloys, was very thin. Thus, the silica layers in the SiO_2/Pt–Co/CB (973 K) catalysts would not prevent the diffusion of oxygen molecules and protons onto Pt–Co alloy surface. Anderson et al. reported that modification of Pt/CB electrocatalysts with silica aerogel improved their catalytic activity for the oxidation of methanol, because the addition of silica aerogel into Pt/CB permitted facile mass transportation of methanol [47]. In contrast, we did

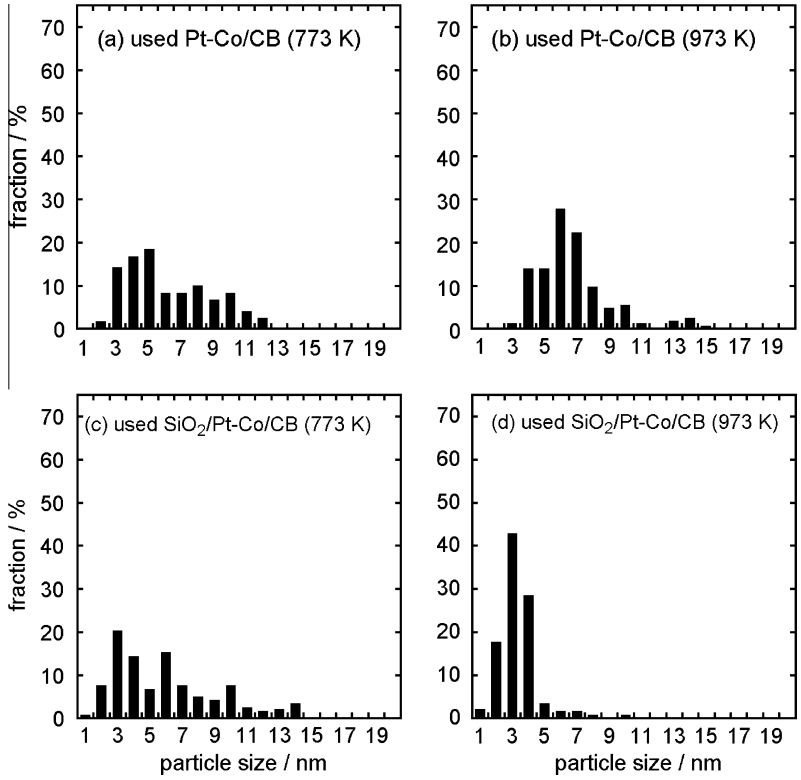

Fig. 10. Particle size distribution for Pt–Co/CB and SiO_2/Pt–Co/CB catalysts after 6000 cycles of the potential cycling.

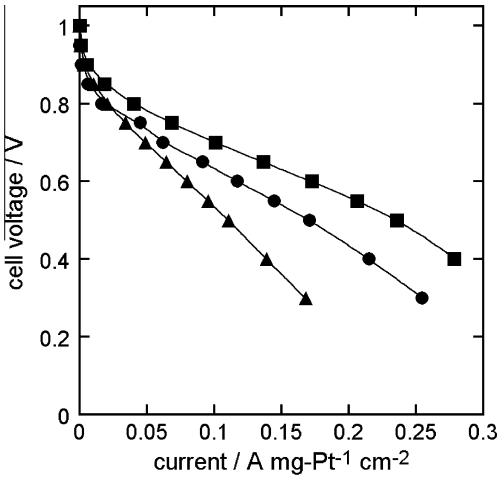

Fig. 11. Polarization curves for the PEFC single cells with fresh Pt/CB (●), Pt–Co/CB (973 K) (▲) and SiO_2/Pt–Co/CB (973 K) (■) catalysts at cathode. Hydrogen (40 ml min^{-1}) for anode and oxygen (40 ml min^{-1}) for cathode were humified at 353 K before feeding into the single cells. The Pt loading in the catalysts at cathode and anode in MEAs was adjusted to 0.2 mg-Pt cm^{-2}.

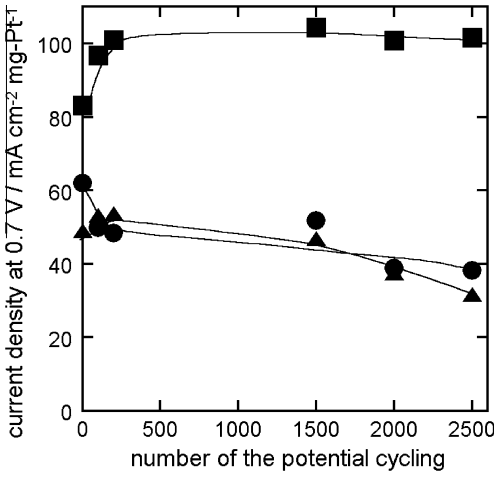

Fig. 12. Change in current density at 0.7 V of cell voltage for the PEFC single cells with Pt/CB (●), Pt–Co/CB (973 K) (▲) and SiO_2/Pt–Co/CB (973 K) (■) catalysts at cathode during the accelerated durability tests.

not observe the improvement in the activity of Pt catalysts for the ORR by coverage with silica layer [22]. The surface area and particle size of the silica aerogel were significantly different from those of silica layer in our catalysts. Thus, we consider that the high activity of SiO_2/Pt–Co/CB (973 K) for the ORR results from a high alloying degree and a small particle size of Pt–Co alloys.

The cell voltage of these PEFC single cells was repeatedly changed between 0.05 and 1.0 V for the accelerated durability test of the catalysts at the cathode as hydrogen and nitrogen gases were fed into the anode and cathode, respectively. Fig. 12 shows the change in catalytic activity for the ORR at the cathode (current density at 0.7 V cell voltage) during the accelerated durability test. The catalytic activity of Pt/CB decreased rapidly during the early stages of the accelerated durability test, and then it decreased slowly with an increase in the number of potential cycles. The catalytic activity of the Pt–Co/CB (973 K) also decreased gradually with an increase in the number of potential cycles. In contrast, the catalytic activity of SiO_2/Pt–Co/CB (973 K) became higher with the number of the potential cycling at early period of the durability test, although the ECSA estimated by CVs for the catalysts slightly decreased during the durability test as shown in Fig. 8. In the measurement of CVs for SiO_2/Pt–Co/CB (973 K) in Fig. 8, ca. 20 cycles of the potential cycling from 0.05 to 1.20 V were carried out to obtain the

reproducible CVs before the durability test of the catalysts by the potential cycling from 0.05 V to 1.0 V. On the other hand, the cell voltage was repeatedly changed from 0.05 to 1.0 V in the durability test using the single cell in Fig. 12. The potential change for the SiO_2/Pt–Co/CB (973 K) would bring about the rearrangement of surface structure in Pt–Co alloys, such as the formation of Pt-rich surface, which causes the increase in the catalytic activity for the ORR. The rearrangement of Pt–Co alloy surface likely occurs more rapidly when the potential of the catalysts increases to 1.20 V. Therefore, the increase in the ECSA of SiO_2/Pt–Co/CB (973 K) could not be observed during the measurement of CVs. After 200 cycles of the potential cycling, the catalytic activity of SiO_2/Pt–Co/CB (973 K) did not change appreciably during the accelerated durability test [27,28,36,48]. The small particle size and high alloying degree of Pt–Co alloys in the SiO_2/Pt–Co/CB (973 K) resulted in the high activity and excellent durability for the ORR.

4. Conclusions

We have covered Pt–Co/CB catalysts with silica layers to inhibit the aggregation of Pt–Co alloy particles during the treatment of the catalysts at high temperatures to allow alloy formation. The coverage of Pt–Co/CB catalysts with silica promoted the formation of Pt–Co alloys with a higher alloying degree and smaller particle size. Thus, the silica-coated Pt–Co catalysts showed high activity and excellent durability for the oxygen reduction reaction. The silica-coating technique is useful for the preparation of various alloy nanoparticle catalysts.

Acknowledgment

This work was supported by a Grant-in-Aid for Scientific Research (B) (No. 20360365) for the Ministry of Education, Culture, Science, Sports and Technology of Japan.

References

[1] G.A. Gruver, R.F. Pascoe, H.R. Kunz, J. Electrochem. Soc. 127 (1980) 1219.
[2] A.C.C. Tseung, S.C. Dhara, Electrochim. Acta 20 (1975) 681.
[3] A. Honji, T. Mori, K. Tamura, Y. Hishimura, J. Electrochem. Soc. 135 (1988) 355.
[4] X. Yu, S. Ye, J. Power Sour. 172 (2007) 133.
[5] E. Antolini, J.R.C. Salogado, E.R. Gonzalez, J. Power Sour. 160 (2006) 957.
[6] V. Jalan, E.J. Tayler, J. Electrochem. Soc. 130 (1983) 2299.
[7] S.J. Mukerjee, Appl. Electrochem. 20 (1990) 537.
[8] B.C. Beard, P.N. Ross Jr., J. Eelctrochem. Soc. 137 (1990) 3368.
[9] T. Toda, H. Igarashi, H. Uchida, M. Watanabe, J. Eelctrochem. Soc. 146 (1999) 3570.
[10] S. Koh, J. Leisch, M.F. Toney, P. Strasser, J. Phys. Chem. C 111 (2007) 3744.
[11] X. Li, H.R. Colón-Mercado, G. Wu, J.W. Lee, B.N. Popov, Electrochem. Solid State Lett. 10 (2007) B201.
[12] G. Wang, T. Takeguchi, E.N. Muhamad, T. Yamanaka, M. Sadakane, W. Ueda, J. Electrochem. Soc. 156 (2009) B1348.
[13] S. Takenaka, Y. Shigeta, E. Tanabe, K. Otsuka, J. Phys. Chem. B 108 (2004) 7656.
[14] M. Min, J. Cho, K. Cho, H. Kim, Electrochim. Acta 45 (2000) 4211.
[15] G. Thamizhmani, G.A. Capuano, J. Electrochem. Soc. 141 (1994) 968.
[16] N. Travitsky, T. Ripenbein, D. Golodnitsky, Y. Rosenberg, L. Burshtein, E. Peled, J. Power Sour. 161 (2006) 782.
[17] Y. Qian, W. Wen, P.A. Adcock, Z. Jiang, N. Hakim, M.S. Saha, S. Mukerjee, J. Phys. Chem. C 112 (2008) 1146.
[18] S.C. Zignani, E. Antolini, E.R. Gonzalez, J. Power Sour. 182 (2008) 83.
[19] S. Takenaka, K. Hori, H. Matsune, M. Kishida, Chem. Lett. 34 (2005) 1594.
[20] S. Takenaka, H. Umebayashi, E. Tanabe, H. Matsune, M. Kishida, J. Catal. 245 (2007) 392.
[21] S. Takenaka, H. Matsumori, K. Nakagawa, H. Matsune, E. Tanabe, M. Kishida, J. Phys. Chem. C 111 (2007) 15133.
[22] S. Takenaka, H. Matsumori, H. Matsune, E. Tanabe, M. Kishida, J. Electrochem. Soc. 155 (2008) B929.
[23] J. Shen, Y. Hu, C. Li, C. Qin, M. Ye, Electrochim. Acta 53 (2008) 7276.
[24] S. Takenaka, T. Arike, H. Matsune, E. Tanabe, M. Kishida, Carbon 46 (2008) 365.
[25] S. Takenaka, T. Arike, H. Matsune, E. Tanabe, M. Kishida, J. Catal. 257 (2008) 345.
[26] A. Ankudinov, B. Ravel, J.J. Rehr, S.D. Conradson, Phys. Rev. B 58 (1998) 7565.
[27] P. Yu, M. Pemberton, P. Plasse, J. Power Sour. 144 (2005) 11.
[28] H.R. Colón-Mercado, B.N. Popov, J. Power Sour. 155 (2006) 253.
[29] S. Takenaka, T. Iguchi, E. Tanabe, H. Matsune, M. Kishida, Carbon 47 (2009) 1251.
[30] H. Schulenburg, E. Müller, G. Khelashvili, T. Roser, H. Bönnemann, A. Wokaun, G.G. Scherer, J. Phys. Chem. C 113 (2009) 4069.
[31] F.H.B. Lima, J.F.R. de Castro, L.G.R.A. Santos, E.A. Ticianelli, J. Power Sour. 190 (2009) 293.
[32] T. Tanaka, H. Yamashita, R. Tsuchitani, T. Funabiki, S. Yoshida, J. Chem. Soc. Faraday Trans. 1 (84) (1988) 2987.
[33] T. Shishido, H. Asakura, F. Amano, T. Sone, S. Yamazoe, K. Kato, K. Teramura, T. Tanaka, Catal. Lett. 131 (2009) 413.
[34] J.A. Horsely, J. Chem. Phys. 76 (1982) 1451.
[35] Y.W. Tsai, Y.L. Tseng, L.S. Sarma, D.G. Liu, J.F. Lee, B.J. Hwang, J. Phys. Chem. B 108 (2004) 8148.
[36] B.J. Hwang, S.M.S. Kumar, C.H. Chen, Monalisa, M.Y. Cheng, D.G. Liu, J.F. Lee, J. Phys. Chem. C 111 (2007) 15267.
[37] E.K. Hlil, R. Baudoing-Savois, B. Moraweck, A.J. Renouprez, J. Phys. Chem. 100 (1996) 3102.
[38] Y.S. Lee, J.Y. Rhee, C.N. Whang, Y.P. Lee, Phys. Rev. B 68 (2003) 235111.
[39] F.J. Lai, L.S. Sarma, H.L. Chou, D.G. Liu, C.A. Hsieh, J.F. Lee, B.J. Hwang, J. Phys. Chem. C 113 (2009) 12674.
[40] A. Witkowska, S. Dsoke, E. Principi, R. Marassi, A.D. Cicco, V.R. Albertini, J. Power Sour. 178 (2008) 603.
[41] S. Takenaka, M. Ishida, M. Serizawa, E. Tanabe, K. Otsuka, J. Phys. Chem. B 108 (2004) 11464.
[42] S. Takenaka, Y. Orita, H. Matsune, E. Tanabe, M. Kishida, J. Phys. Chem. C 111 (2007) 7748.
[43] W. Yu, W. Tu, H. Liu, Langmuir 15 (1999) 6.
[44] W. Li, C. Liang, W. Zhou, J. Qiu, Z. Zhou, G. Sun, Q. Xin, J. Phys. Chem. B 107 (2003) 6292.
[45] E. Antolini, Mater. Chem. Phys. 78 (2003) 563.
[46] H. Matsumori, S. Takenaka, H. Matsune, M. Kishida, Appl. Catal. A: Gen. 373 (2010) 176.
[47] M.L. Anderson, R.M. Stroud, D.R. Rolison, Nano Lett. 2 (2002) 235.
[48] H. Yano, J.M. Song, H. Uchida, M. Watanabe, J. Phys. Chem. C 112 (2008) 8372.